

Synthesizing Adversarial Visual Scenarios for Model-Based Robotic Control

Shubhankar Agarwal* and Sandeep P. Chinchali *

Abstract: Today’s robots usually interface data-driven perception and planning models with classical model-predictive controllers (MPC). Often, such learned perception/planning models produce erroneous waypoint predictions on out-of-distribution (OoD) or even adversarial visual inputs, which increase control cost. However, today’s methods to train robust perception models are largely task-agnostic – they augment a dataset using random image transformations or adversarial examples targeted at the vision model in *isolation*. As such, they may introduce pixel perturbations that are ultimately benign for control. In contrast to prior work that synthesizes adversarial examples for single-step vision tasks, our key contribution is to synthesize adversarial scenarios tailored to multi-step, model-based control. To do so, we use differentiable MPC methods to calculate the sensitivity of a model-based controller to errors in state estimation. We show that *re-training* vision models on these adversarial datasets improves control performance on OoD test scenarios by up to 36.2% compared to standard task-agnostic data augmentation. We demonstrate our method on examples of robotic navigation, manipulation in RoboSuite, and control of an autonomous air vehicle.

1 Introduction

Imagine a drone that must safely navigate using its camera and a learned perception module, such as a deep neural network (DNN). The drone’s perception DNN and planning module output a sequence of waypoints that are tracked by MPC to achieve a low-cost trajectory [1, 2]. However, the drone will often observe weather and terrain conditions that are far from its original image training distribution. In this paper, we ask whether we can automatically synthesize adversarial visual scenarios for multi-step, *model-based* control tasks in order to re-train more robust robotic perception models.

Today’s robust training methods include data augmentation [3, 4], domain randomization [5, 6], and adversarial training [7–9]. These methods add synthetic visual examples by randomly cropping, rotating, or adversarially altering targeted pixels in a training distribution. However, such augmentation methods aim to improve the vision model in isolation and hence are largely *task-agnostic*. While some methods [10–12] perform data augmentation for the ultimate end-to-end control task, the data-augmentation techniques are still task-agnostic, such as using random crops, blur, etc. As such, they often synthesize visual examples that do not adequately affect control-relevant states.

Our work bridges advances in generative models [13, 14], differentiable rendering [15, 16], and differentiable MPC [17]. These advances enable us to synthesize realistic visual scenes from a set of latent, often-interpretable, parameters and calculate their impact on control cost. Our principal contribution is a training procedure (Fig. 1) that efficiently perturbs the latent representation of an image so that we render scenarios that are poor for control, but consistent with naturally-occurring data. Moreover, we can visualize the latent representations of scenes to see how task-driven data augmentation improves the diversity of training examples, resulting in more robust models.

Literature Review: Many perception models are susceptible to adversarial examples [7–9, 18]. For example, the Fast Gradient Sign Method (FGSM) calculates the sensitivity of a pre-trained classifier to distortions in the image input, which guides how we synthesize human-imperceptible pixel changes that cause mis-classifications. However, to the best of our knowledge, there is no work describing how such image perturbations ultimately affect *multi-step, model-based* control.

*Department of Electrical and Computer Engineering (ECE), The University of Texas at Austin, Austin, TX {somi.agarwal, sandeepc}@utexas.edu

Our work is distinct from robust adversarial reinforcement learning (RARL) [19–22]. First, these methods aim to improve a *control* policy, either by perturbing an agent’s dynamics or introducing an adversarial RL agent that physically impedes progress. In contrast, we focus on fixed, model-based controllers (often represented by a convex program), and instead focus on re-training perception models whose state estimates serve as input parameters for convex MPC. To do so, we use differentiable MPC methods [17, 23, 24] to compute the sensitivity of the control cost to erroneous perceptual inputs. As such, we leverage the structure of MPC to efficiently synthesize adversarial inputs as opposed to model-free RARL methods.

As noted earlier, today’s visual data augmentation [4] is largely task-agnostic – random image crops or rotations might alter perception waypoints, but barely affect control cost. Instead, our method leverages the MPC task’s structure to targetedly perturb pixels that are most salient for control. Finally, our work differs from gradient-free Bayesian Optimization [25] methods (e.g., for safety assurances for self-driving cars [26, 27]) since we explicitly leverage the gradient of MPC’s task cost. In light of this prior work, our contributions are as follows:

1. We develop a novel loss function that flexibly trades-off the realism of adversarial examples and their impact on control cost by learning perturbations in a latent visual space.
2. We present a method to automatically synthesize adversarial examples for vision-based MPC.
3. We show that re-training on these synthesized examples leads to better performance on unseen test data than today’s standard task-agnostic data augmentation on diverse scenarios ranging from aerial navigation to arm manipulation in the photo-realistic RoboSuite simulator [28].

2 Problem Statement

We describe our problem using the information flow in our robot learning architecture (Fig. 1).

Differentiable Perception and Planning Modules: The robot’s perception module ϕ_{perc} maps a high-dimensional visual observation s into a low-dimensional scene embedding z , denoted by $z = \phi_{\text{perc}}(s; \theta_{\text{perc}})$. Here, θ_{perc} are parameters of the perception module, such as a DNN. Next, the robot uses the scene embedding z to plan a collision-free trajectory to achieve its task. Often, we can represent a robot’s trajectory by a sequence of waypoints, such as a set of landmark poses in the xy plane for a 2-D planar robot. Then, the differentiable planning module maps scene embedding z and a vector of P past waypoints w_p to a vector of F future waypoints to follow, denoted by $w_F = \phi_{\text{plan}}(z, w_p; \theta_{\text{plan}})$. Here, θ_{plan} are parameters of the differentiable planner. Henceforth, for brevity, we refer to the composition of the perception and planning modules as a task module $w_F = \phi_{\text{task}}(s, w_p; \theta_{\text{perc}}, \theta_{\text{plan}})$, such as the cascaded operation of two DNNs.

Differentiable MPC: Next, the robot must follow the waypoints w_F with minimal control cost, while incorporating physical constraints. Suppose the robot is at some initial state ζ_t and has a planning horizon of F steps. Then, its controller π should map the initial state ζ_t and future waypoints w_F into a sequence of controls from t to $t + F$, denoted by $u_{t:t+F} = \pi(\zeta_t, w_F; \theta_{\text{MPC}})$. Here, θ_{MPC} could represent feedback gains for MPC. Crucially, we define a task (control) cost $J(w_F; \theta_{\text{perc}}, \theta_{\text{plan}}, \theta_{\text{MPC}})$ which depends on the final waypoints the robot tracks w_F . Since the waypoints w_F depend on the previous perception and planning modules, the cost J depends on their parameters too. The MPC task cost J could balance actuation effort and state deviations from a reference trajectory.

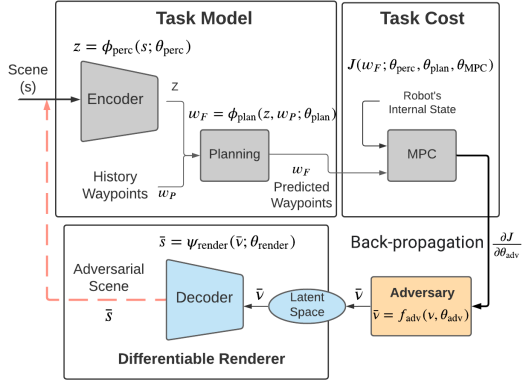


Figure 1: **Differentiable Robot Learning Architecture:** A robot observes an image s , which it maps through an encoder to yield scene embedding z . Given a history of waypoints w_p , a task module (planner) outputs a future set of waypoints w_F to track. Finally, these waypoints are tracked using differentiable MPC that outputs a task cost J . We assume scenes s are rendered by a generative model, such as a differentiable renderer (blue), that maps latent parameters describing a scene v to an image s . **Our key contribution** is to train an adversary (orange) to generate synthetic, but realistic, images \bar{s} that are poor for the current planner and controller. Re-training the planning module on these scenes improves robust performance on OoD data.

Differentiable Rendering Module: This paper analyzes how the ultimate MPC task cost J would increase if the robot observes an adversarial visual input \bar{s} instead of original image s . To do so, we need a process to generate, or render, realistic adversarial scenes \bar{s} . Fortunately, recent progress in generative models and differentiable graphics renderers makes this possible [15, 29]. A differentiable renderer $s = \Psi_{\text{render}}(\mathbf{v}; \theta_{\text{render}})$ generates the robot’s scene s from latent parameters \mathbf{v} that describe the scene and internal parameters θ_{render} of the rendering model. Often, the latent representation \mathbf{v} of scene s could be interpretable and controllable, such as the pose, lighting, and texture of different objects. Without loss of generality, the renderer in our pipeline could also be the decoder in a Variational Autoencoder (VAE) [30] or a Generative Adversarial Network (GAN) [31]. All we require is a differentiable mapping that generates new scenes \bar{s} from latent parameters $\bar{\mathbf{v}}$.

End-to-End Differentiable Architecture: Since every block in Fig. 1 is differentiable, we have an end-to-end differentiable mapping from scene parameters \mathbf{v} to ultimate task cost J . Henceforth, we slightly re-define our notation for the task cost to be $J(\mathbf{v}; \theta_{\text{perc.}}, \theta_{\text{plan}}, \theta_{\text{MPC}})$ to make it explicit that the cost depends on the latent scene representation \mathbf{v} . This is because \mathbf{v} generates scene s , which is mapped to MPC waypoints w_F through the task module. Thus, we can back-propagate the gradient of the MPC task cost J with respect to scene parameters \mathbf{v} to efficiently search for adversarial $\bar{\mathbf{v}}$.

Train/Test Datasets: We must first formalize our dataset notation. A dataset contains N tuples of inputs x and ground-truth labels y denoted by $\mathcal{D} = \{x, y\}_{i=1}^N$. Specifically, each example $x = (s, \mathbf{v}, w_P)$ represents the robot’s scene input s , corresponding latent representation \mathbf{v} from the renderer, and waypoint history w_P . From these, the task model predicts a ground-truth target vector $y = w_F$ of future robot waypoints, which can come from an oracle planner or human demonstrations.

Henceforth, the subscript b in the dataset notation \mathcal{D}_b^a will represent the type of dataset, such as whether it is an original image, from data augmentation, or adversarial training. Likewise, the superscript a will represent if the dataset is from the *train* or *test* distribution. For example, the original training and test datasets are given by $\mathcal{D}_{\text{orig}}^{\text{train}}$ and $\mathcal{D}_{\text{orig}}^{\text{test}}$. The training function TRAIN uses supervised learning to estimate correct waypoints w_F given the scene s . The notation $\theta_{\text{perc.}}^0, \theta_{\text{plan}}^0 \leftarrow \text{TRAIN}(\mathcal{D}_{\text{orig}}^{\text{train}})$ indicates we train the nominal task model parameters on the original training dataset.

For a focused contribution, we consider a scenario where the robot has an MPC controller with fixed parameters θ_{MPC} . Moreover, we have already pre-trained a nominal task model $\{\theta_{\text{perc.}}^0, \theta_{\text{plan}}^0\}$ on original images in $\mathcal{D}_{\text{orig}}^{\text{train}}$. Given these inputs, our problem is to generate an additional dataset $\mathcal{D}_{\text{new}} = \{x, y\}_{i=1}^M$ of M datapoints such that re-training the task model on combined dataset $\mathcal{D}_{\text{orig}}^{\text{train}} \cup \mathcal{D}_{\text{new}}$ will minimize task cost J on a held-out original $\mathcal{D}_{\text{orig}}^{\text{test}}$ and OoD test dataset $\mathcal{D}_{\text{OoD}}^{\text{test}}$. We only consider adding M extra examples to limit training costs. Formally, our problem becomes:

Problem 1 (Data Augmentation for Control) *Given fixed MPC parameters θ_{MPC} , original training dataset $\mathcal{D}_{\text{orig}}^{\text{train}}$, and a priori unknown test datasets, $\mathcal{D}^{\text{test}} = \mathcal{D}_{\text{orig}}^{\text{test}} \cup \mathcal{D}_{\text{OoD}}^{\text{test}}$, find a new dataset $\mathcal{D}_{\text{new}} = \{x, y\}_{i=1}^M$ of size M such that:*

$$\mathcal{D}_{\text{new}}^* = \arg \min_{\mathcal{D}_{\text{new}}} \mathbb{E}_{(s', \mathbf{v}', w_p, w'_F) \sim \mathcal{D}^{\text{test}}} J(\mathbf{v}'; \theta_{\text{perc.}}^*, \theta_{\text{plan}}^*, \theta_{\text{MPC}}),$$

where $\theta_{\text{plan}}^*, \theta_{\text{perc.}}^* \leftarrow \text{TRAIN}(\mathcal{D}_{\text{orig}}^{\text{train}} \cup \mathcal{D}_{\text{new}})$.

It is hard to analytically find the best dataset of M points to minimize task cost on OoD data, since this requires re-training non-convex DNNs. We now describe our adversarial training approach.

3 Adversarial Scenario Generation Algorithm

We aim to generate a dataset of adversarial scenarios \mathcal{D}_{adv} where the original task model performs poorly. Then, by re-training the task model on the joint dataset $\mathcal{D}_{\text{orig}}^{\text{train}} \cup \mathcal{D}_{\text{adv}}$, we hope to improve its robust generalization. To do so, we introduce a differentiable adversary to generate the new dataset \mathcal{D}_{adv} , shown in orange in Fig. 1. The adversary maps the original latent scene representation \mathbf{v} to a perturbed representation $\bar{\mathbf{v}} = f_{\text{adv}}(\mathbf{v}; \theta_{\text{adv}})$, where θ_{adv} are trainable parameters.

Adversary Loss Function: We now introduce a novel loss function to train the adversary f_{adv} . Intuitively, the adversary’s loss function must perturb the latent scene representation \mathbf{v} to $\bar{\mathbf{v}}$ such that the

task cost increases. At the same time, it must ensure that the new rendered scene from \bar{v} is realistic enough to plausibly encounter during real-world testing. Therefore, the following adversarial loss function delicately balances the task cost and distance loss between \bar{v} and v .

```

1 Input:  $\theta_{\text{perc.}}^0, \theta_{\text{plan}}^0, \theta_{\text{MPC}}, \mathcal{D}_{\text{orig}}^{\text{train}}$ 
2 Initialize empty new adversarial dataset  $\mathcal{D}_{\text{adv}} = \{\}$ 
3 for  $(x_i = \{s_i, v_i, w_P\}, y_i) \sim \mathcal{D}_{\text{orig}}^{\text{train}}, 0 \leq i \leq M$  do
4   Init. Adv.  $f_{\text{adv}}(v_i; \theta_{\text{adv}}^0)$  with random  $\theta_{\text{adv}}^0$ 
5   Init. Adv. latent rep.  $\bar{v}^0 = v_i$ 
6   Best Task Loss  $J^* = -\infty$ 
7   Init. Adv. tuple  $(\bar{x}, \bar{y}) = (x_i, y_i)$ 
8   for  $k \leftarrow 1$  to  $K$  do
9     Get Adv. latent params
10     $\bar{v}^k = f_{\text{adv}}(\bar{v}^{k-1}; \theta_{\text{adv}}^{k-1})$ 
11    Render scene  $\bar{s}^k = \psi_{\text{render}}(\bar{v}^k; \theta_{\text{render}})$ 
12    Calculate task cost  $J(\bar{v}^k; \theta_{\text{adv}}^{k-1})$ 
13    Calc. Loss  $L = \mathcal{L}(v_i, \bar{v}^k; \theta_{\text{adv}}^{k-1})$ 
14     $\theta_{\text{adv}}^k \leftarrow \text{BACKPROP}(\theta_{\text{adv}}^{k-1}, L)$ 
15    if  $J(\bar{v}^k, \theta_{\text{adv}}^{k-1}) \geq J^*$  then
16      Update most adv. scene
17       $\bar{x}^k = \{\bar{s}^k, \bar{v}^k, w_P\}$ 
18      Update adv. example  $(\bar{x}, \bar{y}) = (\bar{x}^k, y_i)^a$ 
19       $J^* \leftarrow J$ 
20    end
21  end
22 Return:  $\theta'_{\text{perc.}}, \theta'_{\text{plan}} \leftarrow \text{TRAIN}(\mathcal{D}_{\text{orig}}^{\text{train}} \cup \mathcal{D}_{\text{adv}})$ 

```

Algorithm 1: Adversary Training

^aAs described later in Sec. 5.7, our method is general, and we can either set the label for an adversarial image to be the same label as the original image or an altogether new label. This choice depends on how much the difference between the adversarial scene and the original scene affects task completion and semantic meaning. For example, if an adversarial trajectory changes the original path significantly in motion planning, we can generate new waypoint labels by invoking an offline oracle planner. Suppose we aim to slightly distort an image to emulate different weather and background scenarios, but the target prediction remains the same. In that case, we can use the same label as the original image.

Adversarial Task Cost: Given an original latent scene representation v , the adversary generates an adversarial representation by $\bar{v} = f_{\text{adv}}(v; \theta_{\text{adv}})$. Then, we simply invoke the end-to-end differentiable modules in Fig. 1. Importantly, we use the pre-trained task module parameters $\{\theta_{\text{perc.}}^0, \theta_{\text{plan}}^0\}$ since they will only be re-trained after the adversarial dataset generation procedure. We then calculate the new task cost $J(\bar{v}; \theta_{\text{perc.}}^0, \theta_{\text{plan}}^0, \theta_{\text{MPC}}, \theta_{\text{adv}})$. Importantly, the task cost J depends on the adversary parameters θ_{adv} since they generate perturbed scene representation \bar{v} . For a concise notation, we will represent the task cost $J(\bar{v}; \theta_{\text{perc.}}^0, \theta_{\text{plan}}^0, \theta_{\text{MPC}}, \theta_{\text{adv}})$ as $J(\bar{v}; \theta_{\text{adv}})$, since the parameters $\theta_{\text{perc.}}^0, \theta_{\text{plan}}^0, \theta_{\text{MPC}}$ are fixed.

Consistency (Distance) Loss: To promote generation of plausible adversarial images, we introduce a consistency loss $I(v, \bar{v}) \in \mathbb{R}$. Calculating the distance loss in the *latent space* is a novelty of our loss function based on the observation that similar scenes s and \bar{s} might be very far in the high-dimensional image space due to task-irrelevant pixel variation but might be close in the task-relevant latent space of the renderer ψ_{render} . In our experiments, we use the L_2 norm distance between \bar{v} and v , although our method can accommodate any differentiable distance metric.

Overall Adversarial Loss Function: Finally, our adversarial loss function trades off extra control cost while incentivizing scene realism. During adversarial training, only the adversary’s parameters θ_{adv} are trained while the initial task module parameters are fixed. The distance loss is weighted by κ , which can be flexibly set by a roboticist depending on how adversarial they prefer rendered scenarios to be. The loss to minimize is:

$$\mathcal{L}(v, \bar{v}; \theta_{\text{adv}}) = -J(\bar{v}; \theta_{\text{adv}}) + \kappa I(v, \bar{v}). \quad (1)$$

Adversary Training: Algorithm 1 shows our complete training procedure. The inputs are an original training dataset $\mathcal{D}_{\text{orig}}^{\text{train}}$, fixed MPC parameters θ_{MPC} , and pre-trained task module parameters $\theta_{\text{perc.}}^0, \theta_{\text{plan}}^0$. We randomly sample M datapoints from the training distribution and generate their corresponding adversary by performing gradient descent on our loss function (Eq. 1). Then, we save the most adversarial synthetic examples for subsequent data augmentation. To do so, we use a new adversary for each datapoint rather than training a common adversary for the whole dataset.

On line 3, we iterate through M random samples of the original dataset $\mathcal{D}_{\text{orig}}^{\text{train}}$. Each datapoint x_i is a tuple of input scene s_i , corresponding latent representation v_i , and past waypoints w_P . Lines 4-7 describe how we initialize a *new trainable* adversary for each datapoint. In line 4, we initialize a new adversary f_{adv} with random weights θ_{adv}^0 , which will be specific to the datapoint x_i . Since we train the adversary parameters for K gradient descent steps, we use superscript k to indicate the

adversary’s parameters at training step k . Likewise, we index the new adversarially-generated latent representation at each step k by \bar{v}^k . Finally, in lines 5-7, we initialize a tuple (\bar{x}, \bar{y}) , which will indicate the adversarially generated datapoint and label, with the *original* training dataset’s values.

The crux of our algorithm is in lines 8-18, where we perform K gradient update steps to train the adversary f_{adv} . In each gradient step k , we update the adversary parameters to θ_{adv}^k using loss function \mathcal{L} and back-propagation (lines 9-13). In lines 15-19, we store the adversarial tuple (\bar{x}^k, y_i) if it has higher task cost J than the previous best task cost J^* . Finally, after K gradient steps, we append the best adversarial datapoint (\bar{x}, \bar{y}) to dataset \mathcal{D}_{adv} in line 20. Crucially, we only train the adversary parameters θ_{adv} during dataset generation. At the end, we have generated a new adversarial dataset, which is augmented with the original dataset to re-train the task model parameters $\theta'_{\text{perc}}, \theta'_{\text{plan}}$ on line 22. Our method’s runtime is linear with the size of the dataset but is completely parallelizable since we can train a new adversary for each datapoint in parallel during the *for* loop in line 3.

4 Experimental Results

We now evaluate our method (Alg. 1) on three diverse tasks. The first task is a toy example of 2-D robotic motion planning. The second task concerns manipulation in the RoboSuite [28] environment. Finally, in the third experiment, we make an autonomous aircraft taxi by tracking a runway center-line based on visual inputs in challenging weather conditions.

Adversary Model: We use a linear model for our adversary $f_{\text{adv}}(\mathbf{v}; \theta_{\text{adv}}) = \theta_{\text{adv}} \mathbf{v}$, where $\theta_{\text{adv}} \in \mathbb{R}^{n \times n}$ and $\mathbf{v} \in \mathbb{R}^n$, which was expressive enough to generate realistic scenarios that are poor for control. Our system can easily use more complex DNN adversary models since it is fully differentiable.

Distance Loss and Regularization: We use the L_2 -norm as the consistency loss $I(\mathbf{v}, \bar{\mathbf{v}}) = \|\mathbf{v} - \bar{\mathbf{v}}\|_2^2$ in Eq. (1). As shown in the experiments, the consistency loss weight κ can be flexibly set by the user based on how adversarial they want synthetic examples to be.

Variational Autoencoder (VAE): We use a VAE [30] as the differentiable renderer ψ_{render} from Sec. 2, because of their stable training procedures compared to GANs. Notably, we only use the VAE *Decoder* as the rendering module, which takes parameters \mathbf{v} as input and outputs the image s of the scene. We keep the *Decoder* frozen after training it on the training datasets.

Differentiable MPC: All tasks use the task cost $J(w_F)$ for an MPC problem with quadratic costs and linearized dynamics constraints, as shown in Appendix 5.3. Our key step is to calculate the sensitivity of the task cost J to adversarial perturbations in the image s in order to train the adversary. To do so, we use the PyTorch CVXPY LAYERS library [32] to calculate the gradient of MPC’s solution and task cost (a convex program) with respect to its problem parameters (i.e., waypoint predictions w_F). Then, we back-propagate through the differentiable pipeline in Fig. 1 to compute the gradient of MPC’s task cost with respect to the adversary’s parameters.

Architectures: All experiments use DNNs for all modules in Fig. 1 except model-based control and the adversary. The perception module ϕ_{perc} is a convolutional VAE *Encoder* that maps image s to an embedding z used by the planner. For the planner, we achieved success with simple multi-layer perceptrons (MLPs) that output waypoints, such as locations for the arm to reach in manipulation or desired poses for the aircraft. Our algorithm is agnostic to the type of deep network since it aims to improve any general, differentiable task model. Further training/model details are in Appendix 5.4.

Datasets and Benchmarks: We compare task models trained on the following datasets:

1. ORIGINAL: The task model (perception and planning model) is *only* trained on $\mathcal{D}_{\text{orig}}^{\text{train}}$.
2. DATA ADDED: We add more training examples from the same (or very similar) distribution as the original training dataset, denoted by $\mathcal{D}_{\text{add}}^{\text{train}}$. This tests whether more examples are necessary to achieve better performance. The task model is then trained on the union of the original and added dataset, denoted by $\mathcal{D}_{\text{add}}^{\text{train}} \cup \mathcal{D}_{\text{orig}}^{\text{train}}$.
3. DATA AUGMENTATION: We apply standard *task-agnostic* data augmentation to the original training data. For image inputs s , we applied random contrast, random brightness, and random blur. The augmented dataset is denoted by $\mathcal{D}_{\text{aug}}^{\text{train}}$ and we re-train the task model on $\mathcal{D}_{\text{aug}}^{\text{train}} \cup \mathcal{D}_{\text{orig}}^{\text{train}}$.
4. CURL: CURL[33] uses contrastive learning and standard data augmentation techniques for targeted feature extraction, leading to faster training and robust feature learning (Sec. 5.6).

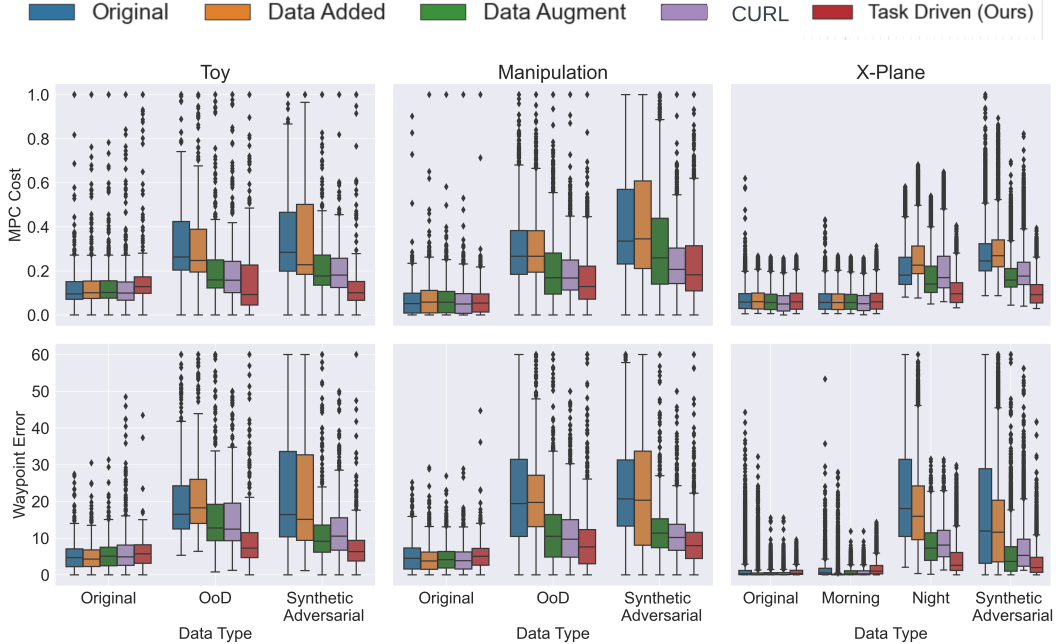


Figure 2: **Benefits of Task-Driven Data Augmentation for Simple 2D Motion Planning, Robot Manipulation and X-Plane Dataset:** We show the MPC task cost J (top) and MSE for waypoint predictions (bottom) for all training schemes on held-out test environments. The x-axis shows different test conditions, and lower task cost and waypoint MSE (y-axis) are better. Our TASK DRIVEN scheme (red) works on par with other task models on the *Original* test data for both metrics and experiments. However, it significantly outperforms other task models on challenging scenarios in the *out-of-distribution (OoD)* dataset (*Night* images for X-Plane), and *Synthetic Adversarial* test datasets. We beat the baselines of task-agnostic data augmentation (green) and CURL (purple), which often apply image augmentations that are ultimately benign for MPC. The DATA ADDED training has high variance on OoD and Adversarial datasets since it overfits to the *Original* dataset.

5. **TASK DRIVEN (Ours):** We use Alg. 1 to synthesize adversarial dataset $\mathcal{D}_{adv}^{train}$ and then re-train the task model on $\mathcal{D}_{adv}^{train} \cup \mathcal{D}_{orig}^{train}$.

Diverse Robotic Tasks: We visualize all model-based robotic tasks in Fig. 4. We use MPC with quadratic costs and linearized robot dynamics in all the experiments. We use linear obstacle avoidance constraints, calculated by drawing perpendicular hyperplanes from the obstacles, discussed further in Appendix 5.3. **Toy 2-D Planning:** In this task, a robot must navigate around obstacles (large ellipsoids) to reach a goal location (green star) using only images s of the 2-D workspace. The planning module learns to output waypoints w_F that mimic a Frenet Planner [34], which are tracked by MPC. The renderer parameters v control the size and location of obstacles in image s . The OoD test dataset consists of larger, more varied obstacles with a different distribution than those in the training dataset. **RoboSuite Manipulation:** A Franka Emika Panda arm [35] needs to pick up a blue ball while avoiding red boxes. The robot observes images s from an overhead camera, and the planning module outputs a collision-free trajectory with waypoints w_F . Then, MPC tracks the trajectory in task-space using the RoboSuite joint controller [35]. The OoD test dataset consists of larger red boxes randomly placed in the scenario compared to those in the training dataset. **X-Plane Aerial Navigation:** This scenario is inspired by academic work for the DARPA Assured Autonomy program [36–39]. An airplane passes images s from a wing-mounted camera into a perception model that estimates its distance and heading angle relative to the center-line of a runway. Then, it uses differentiable MPC to track waypoints w_F that approach the runway center-line. We use a standard benchmark dataset for robust perception [37–39] from the photo-realistic X-Plane simulator [40], consisting of images from the plane’s camera in diverse weather conditions and aircraft poses. Importantly, we test whether a perception model trained on only bright afternoon/morning conditions generalizes to OoD night test scenarios. We also used the Frenet Planner [34] to generate ground truth waypoints of the adversarially synthesized scenarios for Toy 2-D Planning and RoboSuite.

We first trained a VAE on all three domains on all the datasets. Next, we trained the task model (perception and planning models) for a subset of training data defined in Sec. 4. Due to space limits,

we provide further implementation details in Appendix 5.4 and the MPC task cost in Eq. 2. We now evaluate the performance of all training schemes on OoD test datasets. All the results presented are run for 5 random seeds and between 2.5 – 10k test images per dataset (see Appendix).

Domain	Dataset	Avg MPC Cost Difference (%)	Avg Waypoint Error Difference (%)
Toy	$\mathcal{D}_{\text{OoD}}^{\text{test}}$	33.6%	66.1%
	$\mathcal{D}_{\text{adv}}^{\text{test}}$	49.9%	51.5%
Manipulation	$\mathcal{D}_{\text{OoD}}^{\text{test}}$	29.1%	37.1%
	$\mathcal{D}_{\text{adv}}^{\text{test}}$	36.2%	32.8%
X-plane	$\mathcal{D}_{\text{night}}^{\text{test}}$	36.2%	89.2%
	$\mathcal{D}_{\text{adv}}^{\text{test}}$	41.7%	69.1%

Figure 3: **TASK-DRIVEN vs DATA AUGMENTATION schemes for MPC Costs and Waypoint Error:** We compare the percentage improvement in the Avg. MPC cost and Avg. Waypoint Error for the test OoD and synthetic adversarial test datasets. On all domains, our TASK-DRIVEN scheme performs significantly better than DATA AUGMENTATION.

Results: Our experiments show that training the task model with additional adversarial data using Alg. 1 reduces the task cost J and the mean-squared error (MSE) for waypoint prediction compared to all benchmarks. Finally, we visualize how our rendered scenarios are adversarial and realistic.

Quantitative Results: Fig. 2 (top) shows the MPC task cost for all training schemes on test datasets. On the original test dataset, our TASK-DRIVEN scheme (red) performs on par with the ORIGINAL (blue) scheme and slightly worse than the DATA-ADDED (orange), DATA AUGMENTATION (green) and CURL (purple) schemes. The DATA-ADDED scheme’s performance is expected because it is trained on more original data than our TASK-DRIVEN scheme, which allows it to perform slightly better on the original test dataset. However, the key benefits of our approach are shown on the synthetic adversarial test dataset and held-out OoD dataset (real X-Plane night images). We run Alg. 1 on the held-out original test dataset to generate unseen adversarial images which form the synthetic adversarial test dataset. As shown in Fig. 2 (bottom), these benefits arise because our TASK-DRIVEN scheme achieves lower waypoint prediction MSE than competing benchmarks. While all methods perform similarly on the original test dataset, the key gains of our scheme are on the adversarial test dataset and held-out OoD dataset (night images for X-Plane). We compare our TASK-DRIVEN scheme (red) with DATA AUGMENTATION in Table 3, and Table 6 shows the cost differences are statistically significant with a Wilcoxon p-value less than 10^{-4} . Even though the CURL scheme performs best on the original test dataset, it fails to generalize to the test OoD dataset. This is not surprising even though it learns comparably better on the original training dataset; nothing is helping CURL generalize better to the OoD dataset. Additionally, CURL’s performance is similar to DATA AUGMENTATION, since both these methods are exposed to similar augmentation during training.

Qualitative Results: Fig. 4 (bottom row) shows a challenging adversarial scenario that is automatically synthesized by our method in dataset $\mathcal{D}_{\text{adv}}^{\text{train}}$ for the corresponding original training example from $\mathcal{D}_{\text{orig}}^{\text{train}}$ (top row). For the toy planning scenario and manipulation task, our training scheme brings obstacles closer to the robot’s originally intended waypoints and path, making it harder to find a collision-free path. Naturally, this increases the task cost since the robot has to make wider turns and swerves. Specifically, for the manipulation task, the adversary moves red obstacles around the blue target to make it harder to reach and decreases the target size. For the X-Plane scenario, our training scheme learns to blur the runway center-line to emulate a foggy condition, leading to higher waypoint prediction error and task cost. Therefore, rather than augmenting our dataset with well-understood training scenarios, our scheme targetedly adds challenging scenarios that make the model more robust. Finally, Fig. 5 shows the relative distance between different test datasets’ latent representation in the X-Plane renderer when projected in a 2D space using the t-SNE method [41]. Interestingly, our task-driven scheme can add synthetic data points (yellow) that emulate and anticipate the OoD night distribution. However, points added by standard data augmentation (pink) do not overlap much with the night data (green), explaining why the benchmark generalizes poorly.

Limitations: We note that (only for the X-Plane experiment), the original VAE renderer was trained on the whole training dataset. For example, the renderer for the X-Plane experiment was trained on night training images so that the VAE could render a night scene in the first place. However, the initial perception and planning models were never exposed to a single night (OoD) image and were strictly trained on only the original afternoon training data. This scenario is practically motivated. Consider a state-of-the-art differentiable renderer that can map a continuum of scene parameters v to scenes s .

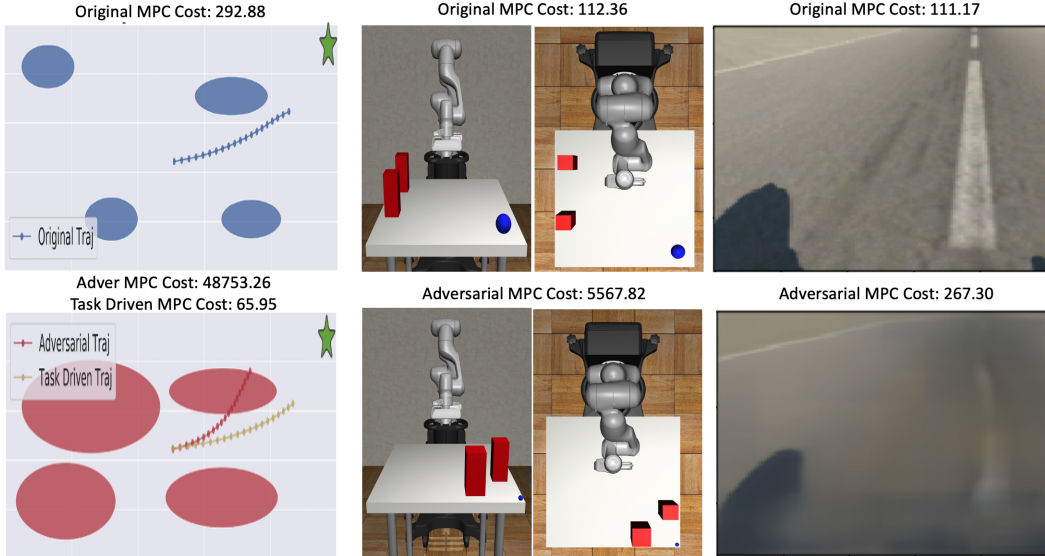


Figure 4: **Synthesized Adversarial Scenarios:** The top row contains images from the original dataset with the corresponding MPC task cost if the predicted waypoints were correctly followed. The bottom row shows the corresponding adversarial scenario generated by our method. As expected, they lead to higher MPC costs by introducing obstacles near a goal or obfuscating the runway center-line. Figs. 11-13 show more examples.

An infinite number of possible images can be generated from the continuous latent space. However, due to compute limits, we can only train the task model on a finite set of scenes \mathcal{V} from a specific training distribution. Thus, we can use our method to automatically and efficiently find new scenes to maximally improve the perception model. Crucially, we must be able to render these new scenes, which is possible with a differentiable renderer. Since we did not have a differentiable renderer for the X-Plane experiment, we used a VAE and ensured it could generate an OoD night image via pre-training for the night class. Additionally, for the cases where the same labels as training cannot be used (Toy Example and Manipulation), our method relies on an offline planner to label the adversarial scenarios. We discuss the labeling procedure further in Sec. 5.7.

Conclusion: This paper presents a principled method to automatically synthesize adversarial scenarios tailored to model-based robotic control. Our key contribution is to compute the sensitivity of MPC to perception errors, which in turn guides better synthesis of adversarial scenarios and robust generalization in state-of-the-art robotic simulators. Our method can benefit applications like self-driving cars by automatically synthesizing rare, OoD scenarios before costly testing and data collection on physical platforms. In future work, we plan to provide theoretical guarantees for an illustrative example with a linear adversary, simple linear renderer/scene generator, and linear MPC control problem. Finally, we plan to test the generalization ability of our approach on a real robot operating in OoD lighting, weather, and terrain conditions.

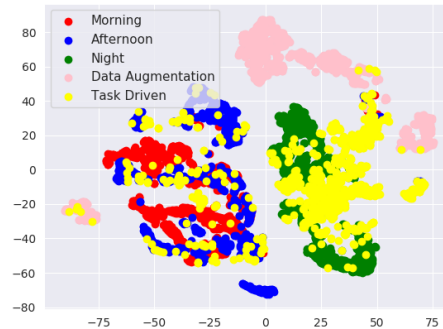


Figure 5: **X-Plane VAE Latent Space Visualization:** We visualize the latent representation $z = \phi_{\text{perc.}}(s; \theta_{\text{perc.}})$ for each test dataset of scenes s after performing dimensionality reduction using t-SNE [41]. The scenes generated by our task-driven method (yellow) are very close to the OoD test night dataset (green), which explains why it generalizes so well. However, the scenes from standard data augmentation (pink) are far from the OoD night scenes, thus explaining why it does not yield generalizable models for control.

Acknowledgements: This material is based upon work supported in part by the Office of Naval Research (ONR) under Grant No. N000142212254. We also gratefully acknowledge the support of the Lockheed Martin AI Center for this research under contract number RPP015-MRA16-005. Any opinions, findings, conclusions, or recommendations expressed in this material are those of the author(s). They do not necessarily reflect the views of ONR or the Lockheed Martin AI Center.

References

- [1] F. Borrelli, A. Bemporad, and M. Morari. *Predictive control for linear and hybrid systems*. Cambridge University Press, 2017.
- [2] E. F. Camacho and C. B. Alba. *Model predictive control*. Springer Science & Business Media, 2013.
- [3] A. Buslaev, V. I. Iglovikov, E. Khvedchenya, A. Parinov, M. Druzhinin, and A. A. Kalinin. Albumentations: Fast and flexible image augmentations. *Information*, 11(2), 2020. ISSN 2078-2489. doi:10.3390/info11020125. URL <https://www.mdpi.com/2078-2489/11/2/125>.
- [4] R. Volpi, H. Namkoong, O. Sener, J. C. Duchi, V. Murino, and S. Savarese. Generalizing to unseen domains via adversarial data augmentation. In S. Bengio, H. Wallach, H. Larochelle, K. Grauman, N. Cesa-Bianchi, and R. Garnett, editors, *Advances in Neural Information Processing Systems*, volume 31. Curran Associates, Inc., 2018. URL <https://proceedings.neurips.cc/paper/2018/file/1d94108e907bb8311d8802b48fd54b4a-Paper.pdf>.
- [5] J. Tobin, R. Fong, A. Ray, J. Schneider, W. Zaremba, and P. Abbeel. Domain randomization for transferring deep neural networks from simulation to the real world. In *2017 IEEE/RSJ international conference on intelligent robots and systems (IROS)*, pages 23–30. IEEE, 2017.
- [6] J. Tobin, L. Biewald, R. Duan, M. Andrychowicz, A. Handa, V. Kumar, B. McGrew, A. Ray, J. Schneider, P. Welinder, et al. Domain randomization and generative models for robotic grasping. In *2018 IEEE/RSJ International Conference on Intelligent Robots and Systems (IROS)*, pages 3482–3489. IEEE, 2018.
- [7] I. J. Goodfellow, J. Shlens, and C. Szegedy. Explaining and harnessing adversarial examples. *arXiv preprint arXiv:1412.6572*, 2014.
- [8] D. Hendrycks, K. Zhao, S. Basart, J. Steinhardt, and D. Song. Natural adversarial examples. In *Proceedings of the IEEE/CVF Conference on Computer Vision and Pattern Recognition*, pages 15262–15271, 2021.
- [9] C. Xie, J. Wang, Z. Zhang, Y. Zhou, L. Xie, and A. Yuille. Adversarial examples for semantic segmentation and object detection. In *Proceedings of the IEEE International Conference on Computer Vision*, pages 1369–1378, 2017.
- [10] S. James, A. J. Davison, and E. Johns. Transferring end-to-end visuomotor control from simulation to real world for a multi-stage task. In S. Levine, V. Vanhoucke, and K. Goldberg, editors, *Proceedings of the 1st Annual Conference on Robot Learning*, volume 78 of *Proceedings of Machine Learning Research*, pages 334–343. PMLR, 13–15 Nov 2017. URL <https://proceedings.mlr.press/v78/james17a.html>.
- [11] D. Kalashnikov, A. Irpan, P. Pastor, J. Ibarz, A. Herzog, E. Jang, D. Quillen, E. Holly, M. Kalakrishnan, V. Vanhoucke, and S. Levine. Scalable deep reinforcement learning for vision-based robotic manipulation. In A. Billard, A. Dragan, J. Peters, and J. Morimoto, editors, *Proceedings of The 2nd Conference on Robot Learning*, volume 87 of *Proceedings of Machine Learning Research*, pages 651–673. PMLR, 29–31 Oct 2018. URL <https://proceedings.mlr.press/v87/kalashnikov18a.html>.
- [12] J. Matas, S. James, and A. J. Davison. Sim-to-real reinforcement learning for deformable object manipulation. In A. Billard, A. Dragan, J. Peters, and J. Morimoto, editors, *Proceedings of The 2nd Conference on Robot Learning*, volume 87 of *Proceedings of Machine Learning*

- Research*, pages 734–743. PMLR, 29–31 Oct 2018. URL <https://proceedings.mlr.press/v87/matas18a.html>.
- [13] T. Daniel and A. Tamar. Soft-intro vae: Analyzing and improving the introspective variational autoencoder. In *Proceedings of the IEEE/CVF Conference on Computer Vision and Pattern Recognition (CVPR)*, pages 4391–4400, June 2021.
- [14] O. Rybkin, K. Daniilidis, and S. Levine. Simple and effective vae training with calibrated decoders, 2021.
- [15] K. Park, A. Mousavian, Y. Xiang, and D. Fox. Latentfusion: End-to-end differentiable reconstruction and rendering for unseen object pose estimation. In *Proceedings of the IEEE Conference on Computer Vision and Pattern Recognition*, 2020.
- [16] H. Kato, D. Beker, M. Morariu, T. Ando, T. Matsuoka, W. Kehl, and A. Gaidon. Differentiable rendering: A survey. *arXiv preprint arXiv:2006.12057*, 2020.
- [17] A. Agrawal, S. Barratt, S. Boyd, and B. Stellato. Learning convex optimization control policies. In *Learning for Dynamics and Control*, pages 361–373. PMLR, 2020.
- [18] N. Akhtar and A. Mian. Threat of adversarial attacks on deep learning in computer vision: A survey. *Ieee Access*, 6:14410–14430, 2018.
- [19] M. Lutter, S. Mannor, J. Peters, D. Fox, and A. Garg. Robust value iteration for continuous control tasks. *arXiv preprint arXiv:2105.12189*, 2021.
- [20] A. Mandlekar, Y. Zhu, A. Garg, L. Fei-Fei, and S. Savarese. Adversarially robust policy learning: Active construction of physically-plausible perturbations. In *2017 IEEE/RSJ International Conference on Intelligent Robots and Systems (IROS)*, pages 3932–3939. IEEE, 2017.
- [21] L. Pinto, J. Davidson, R. Sukthankar, and A. Gupta. Robust adversarial reinforcement learning. In *International Conference on Machine Learning*, pages 2817–2826. PMLR, 2017.
- [22] X. Pan, D. Seita, Y. Gao, and J. Canny. Risk averse robust adversarial reinforcement learning. In *2019 International Conference on Robotics and Automation (ICRA)*, pages 8522–8528. IEEE, 2019.
- [23] A. Agrawal, S. Barratt, and S. Boyd. Learning convex optimization models. *arXiv preprint arXiv:2006.04248*, 2020.
- [24] B. Amos, I. Jimenez, J. Sacks, B. Boots, and J. Z. Kolter. Differentiable mpc for end-to-end planning and control. In *Advances in Neural Information Processing Systems*, pages 8289–8300, 2018.
- [25] Y. Abeyesirigoonawardena, F. Shkurti, and G. Dudek. Generating adversarial driving scenarios in high-fidelity simulators. In *2019 International Conference on Robotics and Automation (ICRA)*, pages 8271–8277. IEEE, 2019.
- [26] J. Wang, A. Pun, J. Tu, S. Manivasagam, A. Sadat, S. Casas, M. Ren, and R. Urtasun. Advsim: Generating safety-critical scenarios for self-driving vehicles. In *Proceedings of the IEEE/CVF Conference on Computer Vision and Pattern Recognition*, pages 9909–9918, 2021.
- [27] S. Feng, X. Yan, H. Sun, Y. Feng, and H. X. Liu. Intelligent driving intelligence test for autonomous vehicles with naturalistic and adversarial environment. *Nature communications*, 12(1):1–14, 2021.
- [28] Y. Zhu, J. Wong, A. Mandlekar, and R. Martín-Martín. robosuite: A modular simulation framework and benchmark for robot learning. In *arXiv preprint arXiv:2009.12293*, 2020.
- [29] N. Ravi, J. Reizenstein, D. Novotný, T. Gordon, W. Lo, J. Johnson, and G. Gkioxari. Accelerating 3d deep learning with pytorch3d. *CoRR*, abs/2007.08501, 2020. URL <https://arxiv.org/abs/2007.08501>.
- [30] D. P. Kingma and M. Welling. Auto-encoding variational bayes, 2014.

- [31] I. J. Goodfellow, J. Pouget-Abadie, M. Mirza, B. Xu, D. Warde-Farley, S. Ozair, A. Courville, and Y. Bengio. Generative adversarial networks, 2014.
- [32] A. Agrawal, B. Amos, S. Barratt, S. Boyd, S. Diamond, and Z. Kolter. Differentiable convex optimization layers. In *Advances in Neural Information Processing Systems*, 2019.
- [33] M. Laskin, A. Srinivas, and P. Abbeel. Curl: Contrastive unsupervised representations for reinforcement learning. *Proceedings of the 37th International Conference on Machine Learning, Vienna, Austria, PMLR 119*, 2020. arXiv:2004.04136.
- [34] M. Werling, J. Ziegler, S. Kammel, and S. Thrun. Optimal trajectory generation for dynamic street scenarios in a frenet frame. In *Proceedings - IEEE International Conference on Robotics and Automation*, pages 987 – 993, 06 2010. doi:10.1109/ROBOT.2010.5509799.
- [35] S. Haddadin, S. Parusel, L. Johannsmeier, S. Golz, S. Gabl, F. Walch, M. Sabaghian, C. Jaehne, L. Hausperger, and S. Haddadin. The franka emika robot: A reference platform for robotics research and education. *IEEE Robotics and Automation Magazine*, pages 2–20, 2022. doi:10.1109/MRA.2021.3138382.
- [36] D. Cofer, I. Amundson, R. Sattigeri, A. Passi, C. Boggs, E. Smith, L. Gilham, T. Byun, and S. Rayadurgam. Run-time assurance for learning-enabled systems. In *NASA Formal Methods Symposium*, pages 361–368. Springer, 2020.
- [37] S. M. Katz, A. Corso, S. Chinchali, A. Elhafsi, A. Sharma, M. Pavone, and M. J. Kochenderfer. Nasa uli aircraft taxi dataset, 2021. Stanford Research Data, <https://purl.stanford.edu/zz143mb4347>.
- [38] S. M. Katz, A. L. Corso, C. A. Strong, and M. J. Kochenderfer. Verification of image-based neural network controllers using generative models. *arXiv preprint arXiv:2105.07091*, 2021.
- [39] A. Sharma, N. Azizan, and M. Pavone. Sketching curvature for efficient out-of-distribution detection for deep neural networks. *arXiv preprint arXiv:2102.12567*, 2021.
- [40] X-plane 11. <https://www.x-plane.com/>.
- [41] G. E. Hinton and S. Roweis. Stochastic neighbor embedding. In S. Becker, S. Thrun, and K. Obermayer, editors, *Advances in Neural Information Processing Systems*, volume 15. MIT Press, 2003. URL <https://proceedings.neurips.cc/paper/2002/file/6150ccc6069bea6b5716254057a194ef-Paper.pdf>.
- [42] W.-C. S. Zhi-Song Liu, L.-W. Wang, C.-T. Li, M.-P. Cani, and Y.-L. Chan. Unsupervised real image super-resolution via generative variational autoencoder. In *IEEE International Conference on Computer Vision and Pattern Recognition Workshop(CVPRW)*, June 2020.
- [43] A. Ramesh, P. Dhariwal, A. Nichol, C. Chu, and M. Chen. Hierarchical text-conditional image generation with clip latents, 2022. URL <https://arxiv.org/abs/2204.06125>.
- [44] P. Dhariwal and A. Nichol. Diffusion models beat gans on image synthesis. In M. Ranzato, A. Beygelzimer, Y. Dauphin, P. Liang, and J. W. Vaughan, editors, *Advances in Neural Information Processing Systems*, volume 34, pages 8780–8794. Curran Associates, Inc., 2021. URL <https://proceedings.neurips.cc/paper/2021/file/49ad23d1ec9fa4bd8d77d02681df5cfa-Paper.pdf>.
- [45] S. Manivasagam, S. Wang, K. Wong, W. Zeng, M. Sazanovich, S. Tan, B. Yang, W.-C. Ma, and R. Urtasun. Lidarsim: Realistic lidar simulation by leveraging the real world. In *IEEE/CVF Conference on Computer Vision and Pattern Recognition (CVPR)*, June 2020.
- [46] Z. Yang, Y. Chai, D. Anguelov, Y. Zhou, P. Sun, D. Erhan, S. Rafferty, and H. Kretschmar. Surfelgan: Synthesizing realistic sensor data for autonomous driving. In *IEEE/CVF Conference on Computer Vision and Pattern Recognition (CVPR)*, June 2020.

- [47] E. Wong and Z. Kolter. Provable defenses against adversarial examples via the convex outer adversarial polytope. In J. Dy and A. Krause, editors, *Proceedings of the 35th International Conference on Machine Learning*, volume 80 of *Proceedings of Machine Learning Research*, pages 5286–5295. PMLR, 10–15 Jul 2018. URL <https://proceedings.mlr.press/v80/wong18a.html>.
- [48] A. Ilyas, S. Santurkar, D. Tsipras, L. Engstrom, B. Tran, and A. Madry. Adversarial examples are not bugs, they are features. In H. Wallach, H. Larochelle, A. Beygelzimer, F. d'Alché-Buc, E. Fox, and R. Garnett, editors, *Advances in Neural Information Processing Systems*, volume 32. Curran Associates, Inc., 2019. URL <https://proceedings.neurips.cc/paper/2019/file/e2c420d928d4bf8ce0ff2ec19b371514-Paper.pdf>.
- [49] A. Madry, A. Makelov, L. Schmidt, D. Tsipras, and A. Vladu. Towards deep learning models resistant to adversarial attacks. In *International Conference on Learning Representations*, 2018. URL <https://openreview.net/forum?id=rJzIBfZAb>.

5 Appendix

The appendix is organized as follows:

1. Subsection 5.1 gives simple steps to use our algorithm for any robot learning problem.
2. Subsection 5.2 presents the Wilcoxon p-values for Table 3.
3. Subsection 5.3 details the Model Predictive Control formulation we used in all our experiments.
4. Subsection 5.4 describes the DNN architectures, training hyper-parameters, and train/test datasets for all experiments. Specifically, Subsections 5.4.1 - 5.4.3 describe the Toy 2D-Planning experiments, RoboSuite Manipulation experiments, and X-plane experiments respectively.
5. Subsection 5.5 provides an ablation study showing how to tune the weight for the consistency loss κ that determines how adversarial rendered scenarios are.
6. Finally, Figs. 11, 12, and 13 depict adversarial examples for all experiments.
7. We have also submitted all the code and will be making it **open-source**.

5.1 Steps to use Task-Driven Training for Robust Robotic Learning

1. Train a VAE (or any generative model) on the training dataset.
2. Train a task model (i.e., perception and planning model) on the training data, $\mathcal{D}_{\text{orig}}^{\text{train}}$. Note that the perception network does not need to be a VAE Encoder. The task model can be any network, such as MLPs, CNNs, or Transformers.
3. Use Alg. 1 to generate a new adversarial synthetic dataset $\mathcal{D}_{\text{adv}}^{\text{train}}$.
4. Retrain the task model on the combined dataset $\mathcal{D}_{\text{orig}}^{\text{train}} \cup \mathcal{D}_{\text{adv}}^{\text{train}}$.

Scaling to the real-world: Scaling to the real world mainly depends on the output quality of the differentiable renderer (VAE in our experiments). Therefore, if the differentiable renderer can generate real-world images, our adversarial learning procedure will be able to find examples that lead to a higher model-based controller cost. Recently, there have been significant improvements in generative models (used as differentiable renders in our work), such as realistic VAEs [42], transformers (DALLE-2) [43], and diffusion models [44], which can be used as the differentiable renderer in our proposed algorithm. Therefore, due to the flexibility of our proposed algorithm, we can plug in any generative model to generate adversarial scenarios for more realistic and unstructured environments.

Self-driving cars can be a real-world use case of our method. LidarSim [45] and SurfelGan [46] are generative models to synthesize realistic self-driving scenarios, trained on a vast amount of self-driving scenarios (Waymo and Uber datasets). Using our proposed method, we can use these differentiable simulators as differentiable renderers to synthesize new adversarial scenarios.

5.2 Wilcoxon p-values

The difference between standard data augmentation and our task-driven approach is **statistically significant** for both control cost and waypoint error with a Wilcoxon p-value much below 0.01.

Domain	Dataset	Avg MPC Cost		Avg Waypoint Error	
		Difference	Wilcoxon p-value	Difference	Wilcoxon p-value
Toy	$\mathcal{D}_{\text{OoD}}^{\text{test}}$		$1e^{-4}$		$1e^{-4}$
	$\mathcal{D}_{\text{adv}}^{\text{test}}$		0		$1e^{-4}$
Manipulation	$\mathcal{D}_{\text{OoD}}^{\text{test}}$		$1e^{-4}$		$1e^{-4}$
	$\mathcal{D}_{\text{adv}}^{\text{test}}$		0		$1e^{-4}$
X-plane	$\mathcal{D}_{\text{night}}^{\text{test}}$		0		$1e^{-4}$
	$\mathcal{D}_{\text{adv}}^{\text{test}}$		0		$1e^{-4}$

Figure 6: **TASK-DRIVEN vs DATA AUGMENTATION schemes for MPC Costs and Waypoint Error Wilcoxon P-values:** We present the corresponding Wilcoxon p-values for Table 3.

5.3 MPC Cost Functions

Toy 2-D Planning and X-Plane: *Differentiable Model Predictive Control (MPC):* The planning module provides the MPC controller with a waypoint vector w_F for F future timesteps to track. The robot’s state at discrete time t is denoted by $\zeta_t \in \mathbb{R}^{4 \times 1}$, defined as $\zeta_t = \{l_x, l_y, v, \theta\}$ for both experiments. Here, l_x and l_y are the robot’s x, y location in meters, v is the speed in meters/sec, and θ is the robot’s heading angle in radians. The robot’s control input at time t is defined as $u_t = \{a, \gamma\}$, where a is the robot’s acceleration in m/s^2 and γ is the robot’s steering input in radians/sec.

Our main goal is to formulate the task cost $J(w_F)$, which is a standard quadratic cost penalizing state deviations and control effort. Namely, $\mathbf{Q} \in \mathbb{R}^{4 \times 4}$ is the state cost matrix and $\mathbf{R} \in \mathbb{R}^{2 \times 2}$ is the control cost matrix. The matrices $\mathbf{A} \in \mathbb{R}^{4 \times 4}$ and $\mathbf{B} \in \mathbb{R}^{4 \times 2}$ define the robot’s dynamics. For the toy 2-D planning experiment, we use standard double integrator dynamics while the X-Plane experiment uses linearized unicycle dynamics, which is common for experiments on the TaxiNet DARPA Assured Autonomy Dataset [38]. The robot has box control constraints $u_{min} \leq u_t \leq u_{max}$ bounding the minimum and maximum acceleration and steering angle. Likewise, box state constraints $\zeta_{min} \leq \zeta_t \leq \zeta_{max}$ define limits on the velocity and linear obstacle avoidance constraints. These constraints, used only in our first motion planning example, were calculated by drawing perpendicular hyperplanes from the obstacles. Given a set of F future waypoints $w_F = \{w_0, w_1, \dots, w_{F-1}\}$ for a planning horizon starting at $t = 0$, our MPC task cost and problem become:

$$\begin{aligned} \min_{\zeta_{0:F}, u_{0:F-1}} J(w_F) &= \sum_{t=0}^F (w_t^\top - \zeta_t^\top) \mathbf{Q} (w_t - \zeta_t) + \sum_{t=0}^{F-1} u_t^\top \mathbf{R} u_t \\ \text{such that } \zeta_{t+1} &= \mathbf{A} \zeta_t + \mathbf{B} u_t \\ u_{min} &\leq u_t \leq u_{max} \\ \zeta_{min} &\leq \zeta_t \leq \zeta_{max}. \end{aligned} \tag{2}$$

RoboSuite Manipulation: The MPC problem is discussed in Subsec. 5.4.2.

5.4 Experiment Details

5.4.1 Illustrative Toy Example: 2D Obstacle Avoidance.

We now introduce a simple task where a planar 2-D robot has to navigate around obstacles to reach a goal location, as pictured in Fig. 7. This experiment demonstrates how adversarial training creates more challenging scenarios for the task model to plan in. Furthermore, we quantitatively show that a task model trained on adversarial scenarios $\mathcal{D}_{adv}^{train}$ learns to avoid collisions more successfully and with lower control cost compared to standard training procedures.

Visual Input: The input to the 2-D planar robot is a 100×100 grey-scale image s of the scene, including obstacles and the goal g , indicated by a star-shaped marker. Given the sensory input s , the task model $w_F = \phi_{task}(s, w_P)$ is a perception-planning module that outputs a sequence of future waypoints w_F for the robot to navigate. A waypoint w_F is simply a pose the robot must move to in the xy plane. The task model ϕ_{task} uses a history of past waypoints w_P to improve its predictions. The linear MPC task cost is defined in Eq. 2.

Training and Test Datasets: We synthetically created the training $\mathcal{D}_{orig}^{train}$ and the held-out test datasets $\mathcal{D}_{orig}^{test}$ and \mathcal{D}_{OoD}^{test} for the experiments. As shown in Fig. 7, each scenario had randomly generated ellipsoid obstacles with random sizes and locations. The ground truth waypoints $y = w_F$ are generated using a standard Frenet Planner [34] that has full access to all obstacles and start/goal locations for the entire scene. The synthetic dataset contained $|\mathcal{D}_{orig}^{train}| = 7000$ training scenarios and $|\mathcal{D}_{orig}^{test}| = 2200$ test scenarios. A larger similar dataset had $|\mathcal{D}_{add}^{train}| = 10000$ training examples. Another dataset of $|\mathcal{D}_{aug}^{train}| = 10000$ training examples was generated from task-agnostic data augmentation. The synthetic adversarial dataset generated by our method had $|\mathcal{D}_{adv}^{train}| = 10000$ training scenarios and $|\mathcal{D}_{adv}^{test}| = 2200$ adversarial test scenarios. We used $K = 10$ gradient steps in Algorithm 1 to generate the adversarial scenarios. Finally, we also generated a challenging OoD test dataset, \mathcal{D}_{OoD}^{test} , where the ellipsoid obstacles were samples from a different distribution than the original

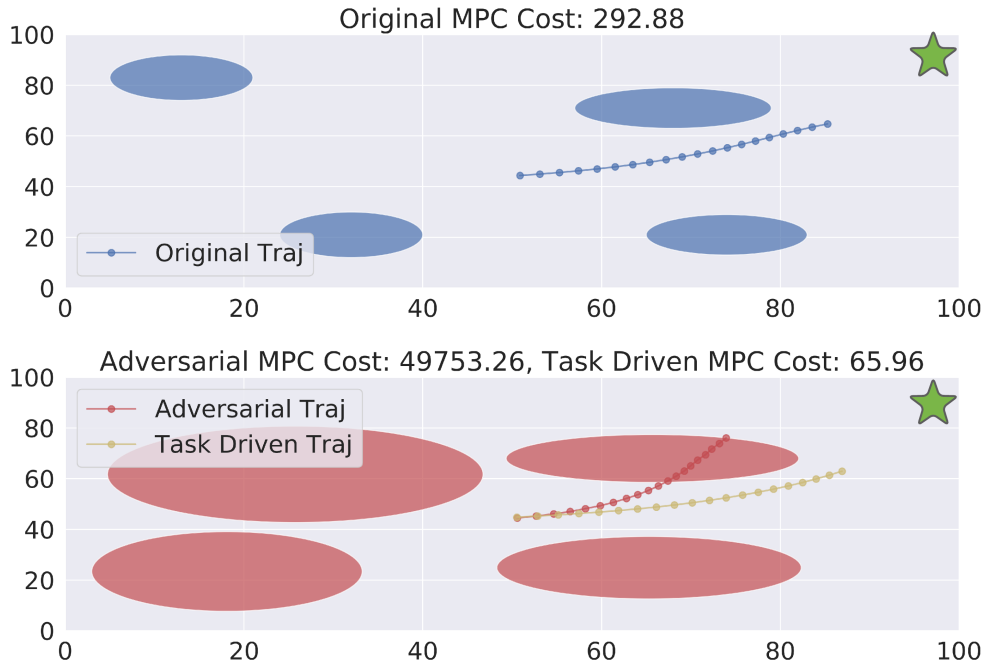


Figure 7: **Our method’s Synthesized Adversarial Scenarios for Toy 2-D Planning:** The robot’s goal is to navigate from a start location at (0,0) to the goal at (100,100) (green star). Original Scene (Top): The blue obstacles (4 ellipsoids) represent the original scene. Adversarial Scene (Bottom): The red obstacles in the bottom are adversarially created using our method for the original scenario above it. The waypoint trajectories (small sequential dots) are generated by the task model for the corresponding scene, and MPC task cost is given in the title. Clearly, the adversarial scenario generates much higher MPC costs by moving the obstacles in the robot’s intended path. Crucially, the waypoint trajectory generated by our *re-trained* TASK DRIVEN scheme (yellow) learns to better avoid the obstacles with lower MPC cost. Fig. 11 shows additional examples.

dataset $\mathcal{D}_{\text{orig}}^{\text{train}}$. Specifically, ellipsoid obstacles were bigger and closer in the OoD test dataset, thus making it hard for the robot to plan.

DNN architectures: We use a history of $P = 10$ past waypoints to predict the next $F = 20$ future waypoints. In this experiment, the VAE Encoder is made up of 3 CNN layers with filter sizes of $[(3, 3), (4, 4), (5, 5)]$, strides of $[1, 2, 2]$, and padding of $[1, 1, 2]$ respectively. Similarly, the decoder is made up of 3 CNN layers with filter sizes of $[(6, 6), (6, 6), (5, 5)]$, strides of $[2, 2, 1]$, and padding of $[2, 2, 2]$ respectively. Rather than hand-tuning a desired weight between reconstruction error and KL divergence with a prior in the VAE loss, we use a σ -VAE [14] which allows for this tuning to happen automatically. We used a VAE with latent size of 20. The VAE is trained with the ADAM optimizer with a learning rate of $1e-3$. The encoder is used for the perception module ϕ_{perc} . and the decoder is used for the differentiable rendering module ψ_{render} . Note that the encoder is re-trained after adversarial scenario generation.

Additionally, for the planning module, ϕ_{plan} is a NN consisting of three fully connected layers with ReLU activation functions with output sizes $[80, 60, 40]$ respectively. The planning module, ϕ_{plan} , is trained with the ADAM optimizer with a learning rate of $1e-3$. The robot’s past waypoints w_P are of length $P = 10$ and the future waypoints w_F are of length $F = 20$. All the planning modules, ϕ_{plan} , were trained for 2000 epochs with early stopping. We experimented with multiple κ values (in loss Eq. 1) and finally used $\kappa = 30$ for the toy experiment. We found our results to be quite robust across a wide range of values κ .

Quantitative results: Table 8 shows the number of scenarios with collisions for all training schemes. Our TASK DRIVEN approach was able to perform as well as the DATA AUGMENTATION, DATA ADDED, and ORIGINAL benchmarks on the original test dataset. Additionally, the TASK DRIVEN approach significantly outperformed the DATA AUGMENTATION scheme by 49%, DATA ADDED

scheme by 67% and ORIGINAL scheme by 69% on the adversarial test dataset \mathcal{D}_{adv}^{test} . Furthermore, our TASK DRIVEN approach outperformed the DATA AUGMENTATION scheme by 15.8%, DATA ADDED scheme by 30.8% and ORIGINAL scheme by 38.6% on the unseen OoD test dataset \mathcal{D}_{OoD}^{test} . Thus, our training scheme TASK-DRIVEN leads to significantly fewer collisions on challenging OoD scenarios.

Figure 8: **Our method improves collision avoidance on challenging motion planning environments:** We show the number of collisions with an obstacle for different training schemes on the original, OoD, and synthetic adversarial test environments. A single collision occurs when the MPC-enacted trajectory intersects an ellipsoidal obstacle. The columns represent how many scenarios of the 2200 test scenarios had even a single collision for held-out test datasets $\mathcal{D}_{orig}^{test}$, \mathcal{D}_{OoD}^{test} and \mathcal{D}_{adv}^{test} respectively. The best performance is bolded and rows correspond to benchmark schemes.

Algorithm	$\mathcal{D}_{orig}^{test}$	\mathcal{D}_{OoD}^{test}	\mathcal{D}_{adv}^{test}
ORIGINAL	389	585	1058
DATA-ADDED	314	552	1044
DATA AUGMENT	321	489	933
TASK-DRIVEN (OURS)	334	422	623

5.4.2 RoboSuite Manipulation

We now introduce the RoboSuite manipulation environment, where the Franka Emika Panda arm has to navigate around red box obstacles to reach a blue ball, as pictured in Fig. 9. This experiment demonstrates how adversarial training creates more challenging scenarios for the task model to plan in. Furthermore, we quantitatively show that a task model trained on adversarial scenarios $\mathcal{D}_{adv}^{train}$ learns to avoid collisions with red boxes more successfully and with lower control cost compared to standard training procedures. The main difference between this domain and the Toy 2-D Planning domain is that inputs scenes for the manipulation task are much more realistic.

Visual Input: The input to the arm is a $64 \times 64 \times 3$ RGB image s of the scene, including red box obstacles and the blue sphere. Given the sensory input s , the task model $w_F = \phi_{task}(s, w_P)$ is a perception-planning module that outputs a sequence of future waypoints w_F for the arm end-effector to navigate. A waypoint w_F is simply a pose the arm end-effector must move to in the xy plane. The task model ϕ_{task} uses a history of past waypoints w_P to improve its predictions. The linearized MPC task space cost is defined in Eq. 2. Specifically, when solving the MPC problem, we treat the middle of the arm-gripper as a point mass trying to reach the blue ball, while avoiding the red box obstacles. After doing this relaxation, we can use the same MPC formulation as shown in Eq. 2. The states ζ_t and the control inputs u_t will relate to the “virtual” point mass at the middle of the arm-gripper. Finally, after obtaining a sequence of MPC waypoints, we used Robosuite’s built-in joint space controller, OSC_POSE, to track MPC’s state trajectory, $\zeta_{0:F}^*$. In all our experiments, the joint space controller was able to generate joint poses to reach the desired task space configuration.

Training and Test Datasets: We create the training $\mathcal{D}_{orig}^{train}$ and the held-out test datasets $\mathcal{D}_{orig}^{test}$ by randomly placing all the red boxes and the blue sphere on a table for the arm to navigate to. The ground truth waypoints $y = w_F$ are generated using a standard Frenet Planner [34] that has full access to all obstacles and start/goal locations for the entire scene. The synthetic dataset contained $|\mathcal{D}_{orig}^{train}| = 20000$ training scenarios and $|\mathcal{D}_{orig}^{test}| = 5000$ test scenarios. A larger similar dataset had $|\mathcal{D}_{add}^{train}| = 30000$ training examples. Another dataset of $|\mathcal{D}_{aug}^{train}| = 20000$ training examples was generated from task-agnostic data augmentation. The synthetic adversarial dataset generated by our method had $|\mathcal{D}_{adv}^{train}| = 10000$ training scenarios and $|\mathcal{D}_{adv}^{test}| = 5000$ adversarial test scenarios. We used $K = 5$ gradient steps in Algorithm 1 to generate the adversarial scenarios. Finally, we also generated a challenging OoD test dataset, \mathcal{D}_{OoD}^{test} , where the red box obstacles were samples from a different distribution than the original dataset $\mathcal{D}_{orig}^{train}$. Specifically, red box obstacles were bigger and closer in the OoD test dataset, thus making it hard for the arm to reach the blue sphere.

DNN Architectures: We use a history of $P = 5$ past waypoints to predict the next $F = 5$ future waypoints. In this experiment, we used a Soft-Intro VAE [13] in order to deal with realistic images. We used a Soft-Intro VAE with a latent size of 500. The Soft-Intro VAE is trained with the ADAM

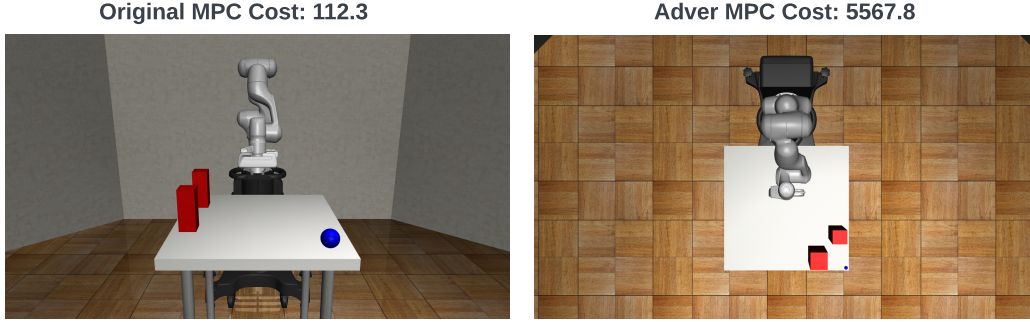


Figure 9: **Our method’s Synthesized Adversarial Scenarios for Robosuite Manipulation:** The arm’s goal is to navigate from a start location to pick up the blue ball. Original Scene (Left): The two red box obstacles and the blue sphere were randomly placed in the the original scene. Adversarial Scene (Right): The red box obstacles are adversarially replaced by our method starting from the original scenario (left). The adversarial scenario generates much higher MPC costs by moving the obstacles in the arm’s intended path and placing them such that arm will have to do big swerves to reach the blue ball.

optimizer with a learning rate of $1e-3$. The encoder is used for the perception module ϕ_{perc} . and the decoder is used for the differentiable rendering module ψ_{render} . Note that the encoder is re-trained after adversarial scenario generation.

Additionally, for the planning module, ϕ_{plan} is a NN consisting of three fully connected layers with ReLU activation functions with output sizes $[1024, 512, 20]$ respectively. The planning module, ϕ_{plan} , is trained with the ADAM optimizer with a learning rate of $1e-3$. The robot’s past waypoints w_P are of length $P = 5$ and the future waypoints w_F are of length $F = 5$. All the planning modules, ϕ_{plan} , were trained for 2000 epochs with early stopping. We experimented with multiple κ values (in loss Eq. 1) and finally used $\kappa = 100$. We found our results to be quite robust across a wide range of values κ .

5.4.3 X-Plane: Autonomous Vision-Based Airplane Taxiing

As shown in Fig. 10, the airplane has a wing-mounted camera and passes the images through a perception model to estimate its distance and heading angle relative to the center-line of a runway. Then, it uses differentiable MPC to navigate to the runway center-line with minimal control cost. We use a public dataset from the photo-realistic X-Plane simulator [40] consisting of images from the plane’s wing-mounted camera in diverse weather conditions and at various poses on the runway. This standard benchmark dataset has been used in recent works on robust and verified perception [37–39].

Visual Input: The input to our “robot” is a 128×128 RGB image s of the runway taken from the right wing. The task model $w_F = \phi_{\text{task}}(s, w_P)$ is a perception-planning module that outputs the desired pose of the airplane w_F , given this sensory input s and a history of waypoints w_P . Specifically, the task model outputs a single waypoint w_F , which is a tuple of the distance to the centerline of runway c and the heading angle θ , denoted by $w_F = (c_i, \theta_i)_{i=0}^F$ for $F = 1$. $w_P = (c_i, \theta_i)_{i=0}^P$ is a history of the $P = 10$ past waypoints which are used to improve the planning model’s predictions. MPC with linearized dynamics (Eq. 2) is used to plan a sequence of controls to navigate to the center-line.

DNN Architectures: In this experiment, we used a Soft-Intro VAE [13] in order to deal with realistic images. We used a Soft-Intro VAE with a latent size of 500. The Soft-Intro VAE is trained with the ADAM optimizer with a learning rate of $1e-3$. The encoder is used for the perception module ϕ_{perc} . and the decoder is used for the differentiable rendering module ψ_{render} . Note that the encoder is re-trained after adversarial scenario generation.

Additionally, for the planning module, ϕ_{plan} is a NN consisting of three fully connected layers with ReLU activation functions with output sizes $[256, 128, 2]$ respectively. The planning module, ϕ_{plan} , is trained with the ADAM optimizer with learning rate of $1e-3$. The robot’s past waypoints w_P are of length $P = 4$ and the future waypoints w_F are of length $F = 1$. All the planning modules, ϕ_{plan} ,

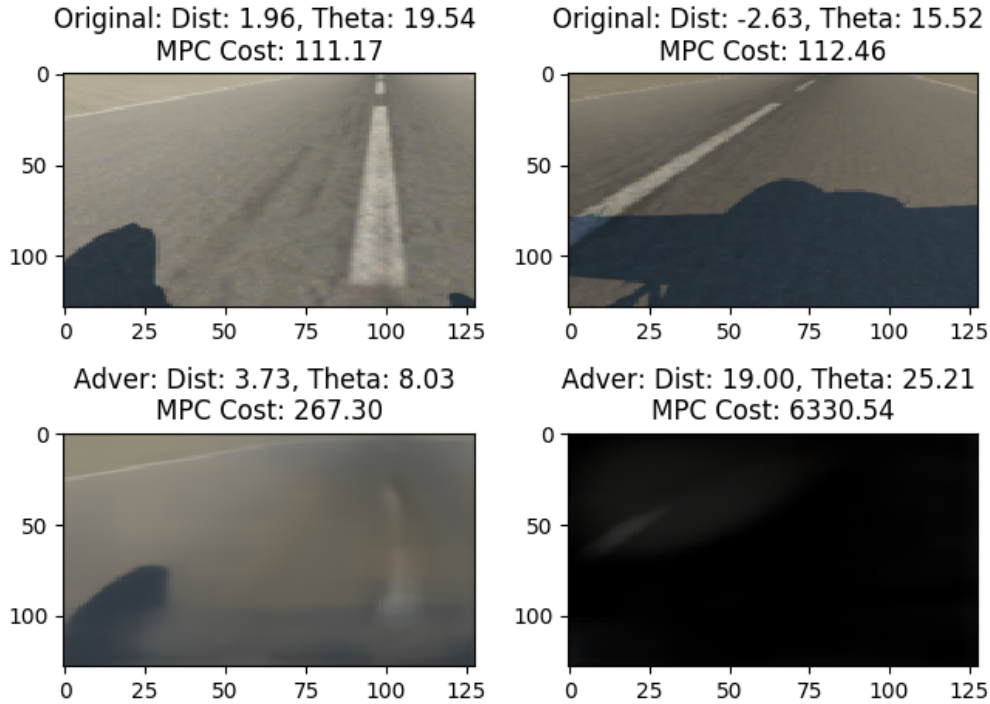


Figure 10: **X-Plane Synthetic Adversarial Scenarios:** The top row contains images from the original dataset with the corresponding ground-truth label waypoint (distance to center-line and heading angle), as well as MPC task cost if this waypoint was correctly followed. The bottom row shows the corresponding adversarial scenario generated by our method. As expected, both the adversarial scenarios lead to higher MPC costs. On the left, the adversary learns to blur the runway center-line to emulate a foggy condition, while the right image emulates an OoD night scenario where only the center-line (top left) is faintly visible. Fig. 13 shows additional examples.

were trained for 2000 epochs with early stopping. We experimented with multiple κ values (in loss eq. 1) and finally used $\kappa = 100$ for the X-Plane experiment.

Images from Diverse Weather Conditions: We will represent the whole X-plane dataset as $\Gamma = \{\mathcal{D}_{\text{afternoon}}, \mathcal{D}_{\text{morning}}, \mathcal{D}_{\text{overcast}}, \mathcal{D}_{\text{night}}\}$, where each dataset corresponds to the subscribed weather condition. Each individual weather dataset in Γ has 44,000 training scenarios and 11,000 testing scenarios. Ground truth waypoints are obtained from the X-Plane simulator.

Our goal is to establish that we can re-train a perception model that robustly generalizes (with good control performance) to OoD weather conditions. To do so, we start with a perception model that is *initially* only trained on afternoon conditions and evaluate its performance on held-out test images across OoD weather conditions. To do so, we will compare 4 different task models ϕ_{task} . The ORIGINAL model is only trained on $\mathcal{D}_{\text{afternoon}}^{\text{train}}$, while the DATA ADDED model is trained on $\mathcal{D}_{\text{add}}^{\text{train}} = \mathcal{D}_{\text{afternoon}}^{\text{train}} \cup \mathcal{D}_{\text{morning}}^{\text{train}}$ since the morning and afternoon are visually similar.

Today’s standard benchmark of task-agnostic data augmentation is trained on $\mathcal{D}_{\text{aug}}^{\text{train}} = \mathcal{D}_{\text{afternoon}}^{\text{train}} \cup \mathcal{D}_{\text{aug}}^{\text{train}}$, where we perform image augmentations (random crops, rotations, and hue alterations) on the original afternoon training data using the open-source Albumentations library [3]. Finally, our TASK DRIVEN model is trained on $\mathcal{D}_{\text{afternoon}}^{\text{train}} \cup \mathcal{D}_{\text{adv}}^{\text{train}}$, where $\mathcal{D}_{\text{adv}}^{\text{train}}$ are adversarial scenarios created using our method applied to the original afternoon training data. We trained the adversary for $K = 15$ steps in Algorithm 1. We quantitatively compare the performance of all benchmark task models on mean task cost J and waypoint MSE on held-out test datasets for each condition, such as afternoon, morning, night (OoD), and synthetic test images ($\mathcal{D}_{\text{adv}}^{\text{test}}$).

5.5 Consistency Loss Weight Ablation Study

This section will show how we can control how adversarial we want the synthetic dataset to be. As a reminder, the loss we used to train the adversary, Eq. 1, contained two parts: the MPC cost of the synthetic adversarial scenario and the consistency loss. The consistency loss calculates the distance between the original scene and the adversarial synthetic scene in the latent space of the renderer. We weigh the consistency loss by a scalar value, κ , which lets users decide how adversarial they want adversarial scenarios to be. From the loss function Eq. 1, it is easy to observe that higher values of κ will make the value of the consistency loss higher than that of the MPC cost. Therefore, the synthetic adversarial scenarios will be less adversarial. Similarly, for lower values of κ , the adversarial scenarios will be more adversarial and thus have higher MPC costs. Fig 14 shows this relation for the Toy 2-D Planning scenario, where we show the MPC Cost (y-axis) for 500 adversarial scenarios for different κ values (x-axis). Fig. 14 clearly shows that as we increase the κ values, the MPC costs of the synthesized adversarial scenarios decrease and are thus less adversarial. We also show that these results are statistically significant in Table 15, with Wilcoxon p-values being less than 0.05 for all cases. We empirically confirm the expected behavior for consistency loss weight κ .

5.6 Comparison with CURL

As an added baseline, we compare our method with CURL [33]. CURL extracts high-level features from raw pixels using contrastive learning and performs waypoint estimation on top of the extracted features (similar to our architecture). Contrastive representations are learned by specifying an anchor observation created using standard augmentation techniques. Specifically, we used random brightness, contrast, blur and crop to create the anchor observations. Then, CURL maximizes/minimizes the agreement between positive/negative pairs in contrastive learning through Noise Contrastive Estimation. CURL explicitly leads to significantly better feature extraction than standard data augmentation and thus speeds up training, converging 2x-3x faster than standard training procedures in our experiments. We used default training parameters for CURL. The learning rate was $3e^{-4}$, and τ (moving average weight) was $5e^{-4}$.

5.7 Adversarial Labels

We now discuss how to generate labels for adversarial images in Algorithm 1. We can use either the same labels or generate new labels depending on how much the adversarial and original scenes differ in terms of task completion and semantics. Here are a few examples.

Case 1: Adversarial Scene Differs Significantly So the Label Changes.

For the Toy 2D Navigation and Robosuite experiments (Left and middle for Fig. 4), the adversary significantly changes the history of waypoints. Thus, we use an “oracle” Frenet Planner [34] to re-plan a collision-avoiding trajectory for the adversarial scenarios and use the new waypoints as ground-truth labels for training.

Case 2: The image is slightly distorted, but the desired waypoint does not change. In X-Plane, the image is only slightly perturbed to emulate new weather or background scenarios due to the consistency loss term. However, the ground-truth location of the runway centerline remains the same since the real pose of the aircraft has not changed. Thus, our method uses the same label for the original and adversarial images. Essentially, our method generates adversarial images that teach the perception model that many possible visual distortions (due to weather/background variation) should map to the same true runway location. Teaching the perception model about these possible visual distortions during training improves its generalization when similar distortions occur in OoD scenarios.

Crucially, we note that using the same labels as the original dataset for image based-tasks is a standard practice in classical adversarial training papers [47–49]. This is because these methods consider small, bounded perturbations on images with the same semantic meaning (same class).

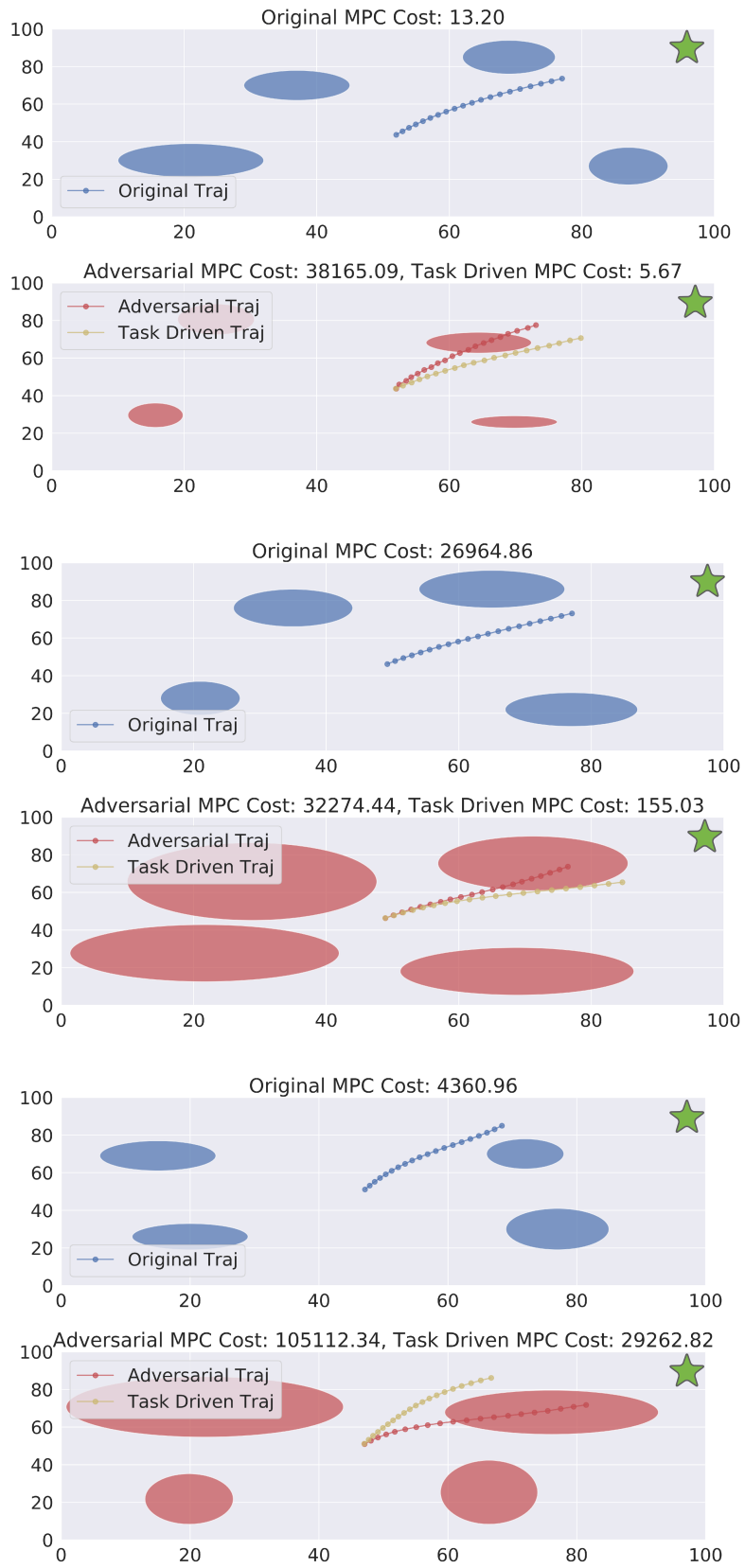


Figure 11: Additional Synthesized Adversarial Scenarios for the Toy 2-D Planning Experiment

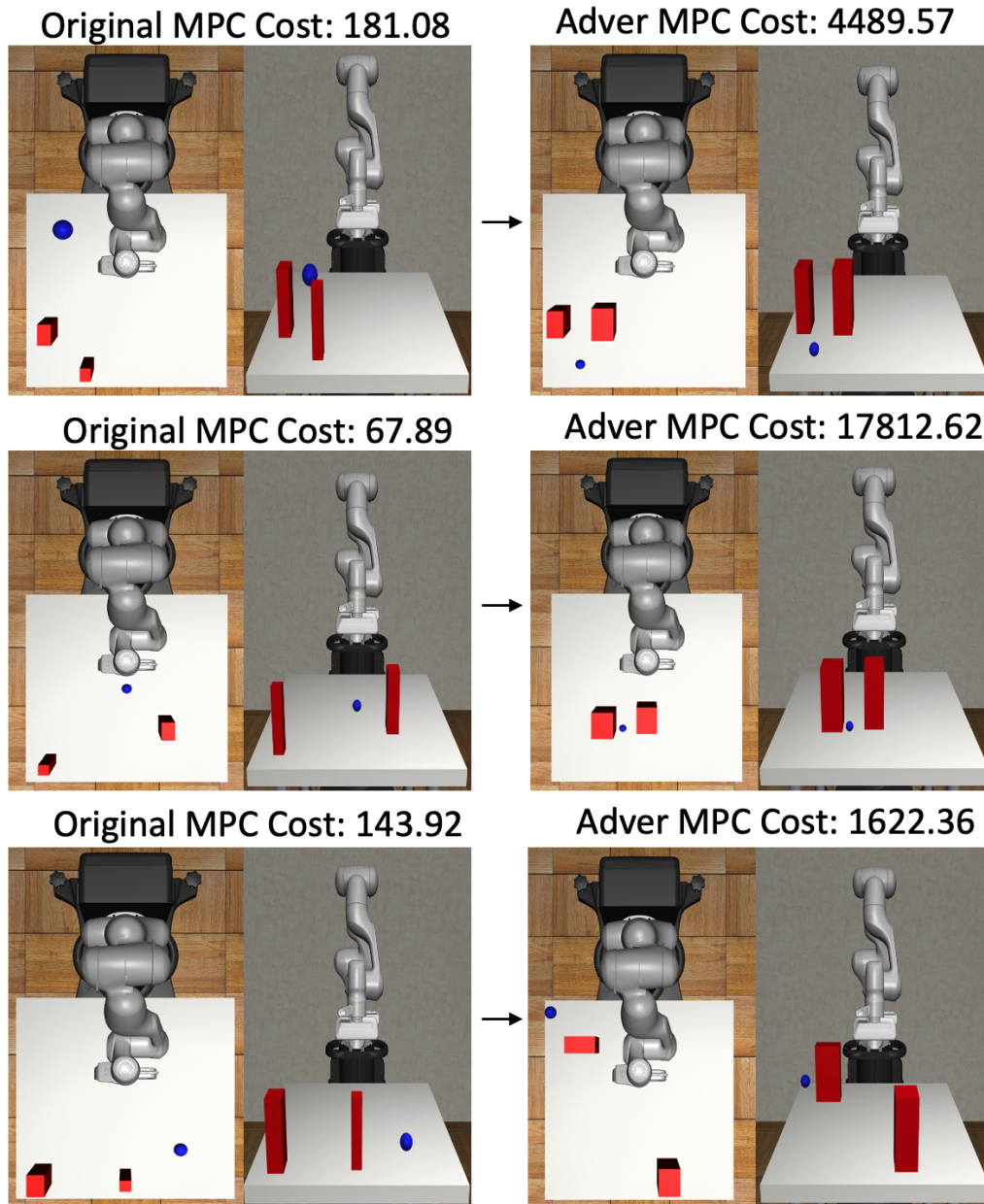


Figure 12: Additional Synthesized Adversarial Scenarios for the Robosuite Manipulation Experiment

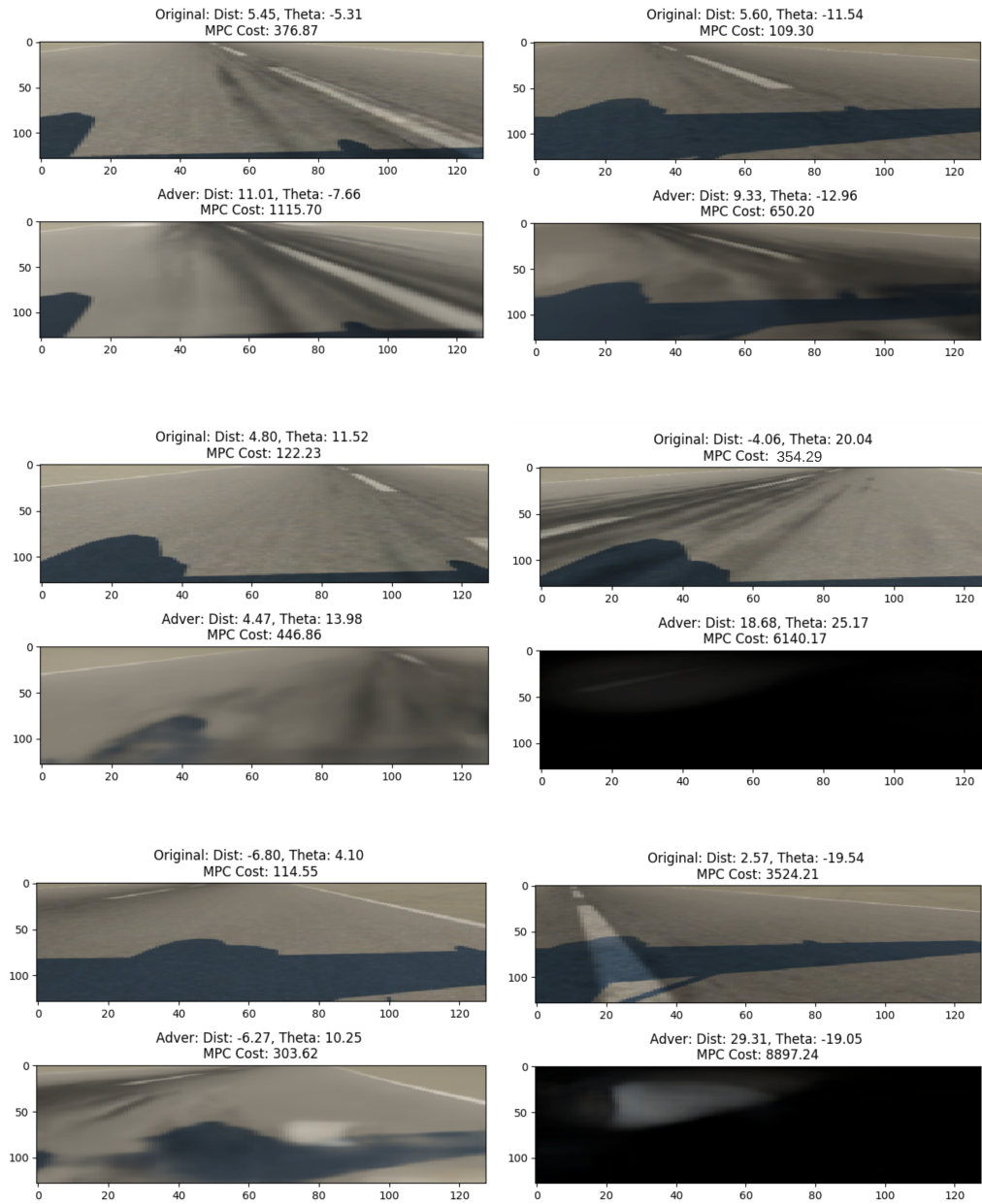


Figure 13: Additional Synthesized Adversarial Scenarios for the X-plane Experiment



Figure 14: **Consistency Loss Weight Ablation Study for Toy 2D Planning:** The figure shows the relation of κ values to the MPC Cost of the corresponding synthesized adversarial scenarios for the Toy 2-D Planning experiment. On the x-axis, we have the κ value used in the adversary loss, Eq. 1, and on the y-axis, we have the corresponding MPC Cost. The plot shows that the user can easily control how adversarial the synthesized scenarios are by tuning the κ value. This plot also demonstrates that our loss function works as desired, as we can see the scenarios with higher κ values have lower MPC costs than scenarios with lower κ values.

Kappa Values	$\kappa = 3$	$\kappa = 30$	$\kappa = 300$
$\kappa = 0.3$	0.042	0.046	0.015
$\kappa = 3$	NA	0.048	0.039
$\kappa = 30$	NA	NA	0.026

Figure 15: **Consistency Loss Weight vs MPC Cost Wilcoxon P-values:** We present the corresponding Wilcoxon p-values for κ ablation study in Fig. 14.